PAPER

Model of resonant high harmonic generation in multi-electron systems

IOP Publishing Journal of Physics B: Atomic, Molecular and Optical Physics
J. Phys. B: At. Mol. Opt. Phys. **50** (2017) 185602 (10pp) https://doi.org/10.1088/1361-6455/aa83d1

Model of resonant high harmonic generation in multi-electron systems

P V Redkin[1] **and R A Ganeev**[2,3]

[1] Department of Physics, Samarkand State University, 15 University Boulevard, Samarkand 140104, Uzbekistan
[2] Faculty of Physics, Voronezh State University, 1 University Square, Voronezh 394006, Russia
[3] Changchun Institute of Optics, Fine Mechanics and Physics, Chinese Academy of Sciences, Changchun 130033, China

E-mail: rdkn_pvl@mail.ru

Received 27 March 2017, revised 9 July 2017
Accepted for publication 3 August 2017
Published 24 August 2017

Abstract

We extend the 4-step analytical model of resonant enhancement of high harmonic generation to the systems possessing resonant transitions of inner-shell electrons. Resonant enhancement is explained by lasing without inversion in a three-level system of ground, excited and shifted resonant states, which are coupled to the fundamental field and its high harmonics. The role of inelastic scattering is studied by simulation of an excited state's population dynamics. It is shown that maximal gain is achieved when the energy shift between the excited state and resonant state is close to the energy of the fundamental photon. To prove the concept we demonstrate the enhancement of harmonics in the In plasma using different pumps.

Keywords: high harmonic generation, laser–plasma, resonant high harmonic generation, laser ablation, MCTDHF, ultrashort pulses

(Some figures may appear in colour only in the online journal)

1. Introduction

High harmonic generation (HHG) in the plasma media produced on the surface of solid targets by laser ablation has been an important part of studies in laser physics over the last 20 years due to the potential applications of short-wavelength coherent radiation in laser holography, lithography, medicine and atto-physics [1]. The only limiting factor of strong-field HHG is its low conversion efficiency to harmonics. There are several ways to increase conversion efficiency (resonance-induced growth of harmonic yield, application of nanoparticles and clusters as the nonlinear media, use of quasi-phase-matching concept, etc). Among them, resonance-induced growth of a single harmonic is one of the simplest and most successful methods [2, 3]. Since the first observation of the phenomenon of resonant HHG in indium (In) plasma [2], some plasma media [3, 4] were identified for the potential enhancement of the single harmonics due to their spectral closeness to ionic transitions possessing strong oscillator strengths.

Analogous attempts for noble gases were reported, which, however, failed to experimentally demonstrate resonant HHG, even in cases when such an enhancement was expected [5–8]. This fact can be attributed to the availability of a much wider range of target materials for plasma HHG compared to a few commonly used gases, which increases the possibility of the resonance of an ionic transition in plasma media with a harmonic wavelength. However, despite the broad range of spectral properties of various laser plasmas, resonant HHG was reported only for a few strong spectral lines in In, Cr, Mn, Sb and As. The resonant enhancement factor varied between 2 and 80 for different laser plasmas. The only difference between the HHG experiments with noble gases and laser plasmas is the fact that laser plasmas are usually singly charged at the moment of interaction with a strong probe pulse, while the noble gases are not. This motivated us to seek a model which ultimately benefits from a sufficient degree of ionization of the media.

Although some possibilities of non-resonant HHG in the intra-atomic dynamics of the electron have been theoretically predicted [9], the experiments [2–4] have shown that the return of the electron to the parent particle predicted by the 3-step model [10] is crucial to the existence of resonant HHG.

As a result, the theories, which do not include the continuum states [5, 11], cannot explain resonant HHG as a direct lasing effect.

Many models describe the enhancement of the HHG yield in the presence of strong intra-atomic resonance as a consequence of the enhanced probability of the bound–bound transition [6, 12–15] or multiphoton ionization [16] at conditions of multiphoton resonance. Multiphoton resonant transitions cannot ensure population inversion, so their impact on resonant HHG originates from an increased ionization probability. Multiphoton ionization can indeed take place even when tunneling ionization is the dominant mechanism. Although the stability of multiphoton resonance in a strong laser field is questionable due to AC Stark shift, any growth of ionization increases the HHG efficiency provided the phase matching conditions are not modified greatly, so multiphoton resonances during ionization should not be discarded from consideration. But the assumption of ionization assisted by multiphoton resonances as the only source of resonant HHG enhancement, especially when combined with the single active electron (SAE) approximation, always predicts the enhancement of a group of harmonics which has not been achieved in typical resonant HHG experiments (see for example [4]).

A semi-classical 4-step model has been suggested [17], which was able to describe most of the properties of resonant HHG in SAE approximation. The additional fourth step in this model is described by cross-section of electron transition to autoionizing (AI) state. This model gives reasonably good qualitative estimates of the efficiencies of resonant HHG for different experimental conditions by substituting experimentally measured decay widths of the resonant levels into a SAE-based analytical formula to account for many-electron effects. There are, however, some uncertainties within this model because SAE approximation does not consider the real structure and dynamics of the intra-atomic electronic structure. Namely, the electrons responsible for the resonant transitions with high oscillator strength definitely belong to the inner shells of the systems in which resonant HHG was experimentally demonstrated. These electrons are in general very unlikely to be ionized directly by tunneling. So the corresponding excited states are not necessarily the AI states of the atomic systems, even if the energy of the resonant transition is close to the ionization energies of the atoms. One should also take into consideration the dressing of higher Rydberg states, which may greatly modify the real AI states of the system.

Another common drawback of all the models of resonant HHG, which assume the population of certain resonant level, is the unclear physical nature of the transition of electrons to the ground state with corresponding emission of coherent radiation at the frequency of a harmonic. If we consider these transitions spontaneous due to the finite lifetime of the resonant level or another laser-dressed state, then the coherence and duration of the resonant radiation will differ greatly compared to non-resonant harmonics. If the process is considered a stimulated emission then the absence of population inversion will lead to a decrease of harmonics near the resonance due to higher probabilities of stimulated absorption even when the degeneracy of the resonantly populated state is high, although the coherence problem of resonant harmonics will be solved. Experimental confirmation of the existence of the spontaneous part of resonant harmonics is an important tool for verification of the proposed approaches. It is still more favorable to consider depletion of the resonantly populated level as a lasing without inversion (LWI) process, which cancels the stimulated absorption cross-section due to interference of two absorption channels in the presence of two fields coupled to the corresponding transitions [18].

In this paper, we introduce the model of resonant HHG in multi-electron systems. Throughout this paper we follow the theory of resonant elastic scattering in the presence of an energetically forbidden inelastic scattering channel in the approximation of strong coupling of two scattering channels. It will be shown that an inelastic scattering channel cannot be completely closed and is extremely important for LWI processes within resonant HHG. However, the nature of the approach is similar to the model of channel closing, which has been successfully applied to studies of anomalous above-threshold ionization (ATI) spectra near ponderomotively upshifted Rydberg states [19, 20]. We also experimentally demonstrate the enhancement of different harmonic orders in the In plasma using the 806, 1431 and 1521 nm pumps.

2. Theory

Considering the two-particle scattering problem, it is useful for particle x (electron for HHG processes) and target A (atomic or ionic core) to denote elastic scattering as

$$x + A \rightarrow x + A \tag{1}$$

and inelastic scattering where the target can be either excited to a bound excited state or a continuum excited state or ionized as

$$x + A \rightarrow x' + A^*. \tag{2}$$

In the approximation of infinitely heavy target A and neglecting identity of electrons for simplicity, the full Hamiltonian of the system ($x \cup A$) can be written as

$$H = \hat{H}_A + \hat{K} + \hat{V} = \hat{H}_0 + \hat{V}, \tag{3}$$

where $\hat{K} = -\frac{\hbar^2}{2\mu}\nabla^2$ is the kinetic energy operator of the particle, $\hat{V} = \hat{V}(\xi, \vec{r})$ is operator of the interaction of the particle with the target, $\hat{H}_A$ is the Hamiltonian of the non-interacting target satisfying the stationary Schrödinger equation

$$\hat{H}_A \Phi_n(\xi) = E_n \Phi_n(\xi);\ n = 0, 1, 2, ... \tag{4}$$

$\Phi(\xi) = \sum \Phi_n(\xi)$ is the expansion of target's wavefunction in the basis of eigenfunctions of a non-interacting target, which forms a full set

$$\langle \Phi_n | \Phi_{n'} \rangle = \delta_{nn'}$$
$$\sum \Phi_n(\xi) \Phi_n^*(\xi') = \delta(\xi - \xi'). \tag{5}$$

Here ξ is a set of inner variables of the target. Note that although the HHG process is non-stationary and highly non-perturbative, the problem of scattering of electrons with a given energy on the target can be solved perturbatively as it contains no expression for the pump field. Note that eigenfunctions actually describe both the bound and continuous states of the non-interacting target, and these eigenfunctions in general do not describe any bound states for the interacting target. The sum sign denotes the summation over the bound state and integration over continuous states. The cross-section of inelastic scattering which excites the target into state n is then given by

$$\left(\frac{d\sigma}{d\Omega}\right)_{|0\rangle\to|n\rangle} = \frac{p_f}{p_i}\left(\frac{\mu}{2\pi\hbar^2}\right)^2 \times |\langle \exp(i\vec{k}_i\vec{r})\Phi_0(\xi)|\ \hat{V}|\exp(i\vec{k}_f\vec{r})\Phi_n(\xi)\rangle|^2 . \quad (6)$$

In the case of $n = 0$, expression (6) gives us the elastic scattering cross-section. Here indices i and f denote initial and final parameters of the scattered electron, $\vec{k}_i = \vec{p}_i/\hbar$, $\vec{k}_f = \vec{p}_f/\hbar$, and according to the energy conservation law

$$\frac{p_f^2}{2\mu} + E_n = \frac{p_i^2}{2\mu}. \quad (7)$$

Where E_n is the energy of resonant inter–atomic transition, expression (6) is the correspondence between the inelastic collision cross-section and the kinetic energy of the electron accelerated by the laser pump field. The perturbation operator $\hat{V}$ is the operator of interaction of the incident electron with the remaining electrons of the atom

$$\hat{V} = \hat{V}(\vec{r};\vec{r}_1,...\vec{r}_z) = -\frac{Ze^2}{r} + \sum_{j=1}^{Z}\frac{e^2}{|\vec{r}-\vec{r}_j|}. \quad (8)$$

Here $\vec{r}$ is the radius-vector from the center of the atom to the incident electron. The second term in this operator assumes significant influence of electronic correlation on the process of resonant HHG, as it has been shown by analysis of influence of precision of representation of electron–electron correlation on resonant HHG in [21]. During the HHG process one should also consider the time-dependent part $\hat{V}(t) = \vec{r}\vec{E}(t)$, this part influences the scattering process only via the AC Stark shift and does not describe the target–particle interaction at all. Using (8), one can outline the total scattering amplitude in the Born approximation as [22]

$$F_{n0}^{(B)}(\vec{k}_f,\vec{k}_i) = -\frac{\mu}{2\pi\hbar^2}\int d^3r e^{i\vec{q}\vec{r}}\int \Phi_n^*(r_1,...,r_Z) \times\left(-\frac{Ze^2}{r} + \sum_{j=1}^{Z}\frac{e^2}{|\vec{r}-\vec{r}_j|}\right) \times \Phi_0(r_1,...,r_Z)d^3r_1...d^3r_Z. \quad (9)$$

Denoting the matrix element by atomic wavefunctions as

$$\langle n|\sum_{j=1}^{Z} e^{i\vec{q}\vec{r}_j}|0\rangle \equiv \int \Phi_n^*(\vec{r}_1,...\vec{r}_Z)\left(\sum_{j=1}^{Z} e^{i\vec{q}\vec{r}_j}\right)\Phi_0(\vec{r}_1,...\vec{r}_Z)d^3r_1...d^3r_Z \quad (10)$$

and using the relation

$$\int e^{i\vec{q}\vec{r}}\frac{1}{|r-r_j|}d^3r = e^{i\vec{q}\vec{r}_j}\int\frac{e^{i\vec{q}(\vec{r}-\vec{r}_j)}}{|r-r_j|}d^3r = \frac{4\pi}{q^2}e^{i\vec{q}\vec{r}_j} \quad (11)$$

we get the final cross-section of elastic scattering in the presence of inelastic scattering and inelastic scattering correspondingly as

$$\frac{d\sigma_{elas}}{d\Omega} = Z^2\left(\frac{d\sigma}{d\Omega}\right)_R |-1 + F_e(\vec{q})|^2, \quad (12)$$

$$\frac{d\sigma_n}{d\Omega} = \frac{p_f}{p_i}\left(\frac{d\sigma}{d\Omega}\right)_R |F_{n0}(\vec{q})|^2. \quad (13)$$

Here $\left(\frac{d\sigma}{d\Omega}\right)_R$ is Rutherford's formula for the differential cross-section of electrons on point unit charge, $F_e(\vec{q})$ is the electronic density form-factor and $F_{n0}(\vec{q})$ is the inelastic electronic form-factor

$$F_e(\vec{q}) = \frac{1}{Z}\int\langle 0|\sum_{j=1}^{Z}\delta(r-r_j)|0\rangle e^{i\vec{q}\vec{r}}d^3r, \quad (14)$$

$$F_{n0}(\vec{q}) = \langle n|\sum_{j=1}^{Z} e^{i\vec{q}\vec{r}_j}|0\rangle,\ |n\rangle \neq |0\rangle. \quad (15)$$

For purposes of resonant HHG, the inelastic electronic form-factor can be simplified to

$$F_{n0}(\vec{q}) = i\vec{q}\langle n|\sum_{j=1}^{Z}\vec{r}_j|0\rangle. \quad (16)$$

In the case of a linearly polarized field, zero initial electron velocity and when the magnetic part is not considered, the accelerated electron is moving one-dimensionally in the polarization direction of the field. So a change of r to z in this case is acceptable as a very good approximation, if the z axis is in the polarization direction of the electric field. In the case of one-dimensional movement of the scattered electron near the return to origin, which is a good approximation for single-color HHG, $\vec{r}_j \to z_j$ and taking into account the expression for the oscillator strength

$$f_{n0} = \frac{2m_e\varepsilon_n}{\hbar^2}\left|\langle n|\sum_j z_j|0\rangle\right|^2,\ \sum_n f_{n0} = Z, \quad (17)$$

one can write the inelastic to elastic cross-section ratio in the conditions of allowed inelastic cross-section

$$\frac{d\sigma_n}{d\sigma_{elas}} = \frac{\frac{p_f}{p_i}q^2\left(\frac{\hbar^2 f_{n0}}{2m_e E_n}\right)}{Z^2\left(-1+\frac{1}{Z}\int\rho_e(\vec{r})e^{i\vec{q}\vec{r}}d^3r\right)},\left(\frac{p_i^2}{2\mu} > E_n\right). \quad (17a)$$

Thus, there is a proportionality of excitation of the inner-shell electron to a higher state by inelastic scattering to oscillator

strength of the considered transition. It can also be shown that optically allowed transitions are excited most strongly in this process

$$\begin{cases} L_n = L_0 \pm 1,\ L_0;\ \Delta L = 0,1; \\ J_n = J_0 \pm 1,\ J_0;\ \Delta J = 0,1 \\ \pi_n = -\pi_0 \end{cases}. \tag{18}$$

This restriction is much weaker than the restriction of single-electron-only transitions $\Delta\ell = \pm 1$, $\Delta m = 0, \pm 1$ and actually allows collective electronic excitations to a metastable resonant state, which may be a collective excitation of inner-shell electrons as well and is most likely responsible for resonant HHG enhancement in C_{60} fullerene laser plasma [23, 24]. However, the state $|n\rangle$ should not be able to experience Auger decay. Transitions responsible for resonant HHG satisfy these conditions. As was pointed out in [16], the excited state can in fact be the origin of emission of other HHG electrons, which then contribute to the harmonics that are close to the resonant one. However, this effect has not been confirmed by experiments, so HHG where the origin state of the accelerated electron is an excited state is not considered important for resonant HHG in this article. The relationship of the probability of spontaneous radiative decay of excited state to coherent HHG photon generation probability, is determined by Einstein coefficients A_{21} and B_{21} and the intensity of non-resonant harmonics as stimulating emission. Following [17], the excited state is populated by inelastic scattering and depopulated via photoionization, where the photoionization cross-section is close to ω (in au). As a result, the resonance is in general sufficiently populated.

In the case of proper conditions for resonant HHG enhancement by stimulated emission being achieved, either by maintaining population inversion between the excited and some other lower state or by phasing out stimulated absorption in the LWI process, the total emitted radiation is given by relation

$$W = \int_\nu q(\nu)\rho_\nu B_{21} \mathrm{d}\nu; \tag{19}$$

$$q(\nu) = \frac{1}{2\pi}\frac{\Delta\nu_{\text{lorentz}}}{(\nu - \nu_0)^2 + \Delta\nu_{\text{lorentz}}^2/4}. \tag{20}$$

In the case of HHG in laser plasmas with relatively low density, the collision of particles is not so frequent so we can consider a variety of relaxation processes. Low-density laser plasma has a concentration in the range of 10^{16}–$10^{18}\,\text{cm}^{-3}$, while the concentration of air at normal conditions is close to $10^{18}\,\text{cm}^{-3}$. One can safely neglect the recombination of accelerated electrons on non-parent ions at such conditions. In addition, the laser–plasma interaction time is too short for the Doppler effects to manifest. So $\Delta\nu_{\text{lorentz}} \approx \Delta\nu_0 = A_{21}/2\pi$. Relation (19) also determines the applicability of relation (6) in [17] due to proportionality to the width of the resonant level. In addition, if resonant width Γ in [17] is assumed to be $\Delta\nu_{\text{lorentz}}$, both models would show a cubic dependence. However, the difference is only visual as the resonant level presented in [7] has a different meaning of resonance inelastic cross-section only because the resonant growth of the elastic cross-section is possible only in conditions where there is no inelastic scattering. In addition, relation (19) has a very strong dependence on the correlation between the spectral width of the corresponding non-resonant harmonic and the transition.

So one should consider the elastic cross-section in the presence of the inelastic cross-section channel closing

$$\left(\frac{p_\text{i}^2}{2\mu} < E_n\right). \tag{21}$$

Separating the contribution of particle and target into the wavefunction of the scattering system to a finite set of field-free eigenfunctions gives

$$\Psi(\xi, \vec{r}) = \sum_n u_n(\vec{r})\Phi_n(\xi), \tag{22}$$

where the so-called channel functions satisfy

$$(\hat{h}_n - E)u_n(\vec{r}) = -\sum_{m\neq n} V_{nm}(\vec{r})u_m(\vec{r}), \tag{23}$$

and the operator of the target–particle interaction in the nth channel is

$$\hat{h}_n = \frac{\hat{p}^2}{2\mu} + E_n + V_{nn}(\vec{r}). \tag{24}$$

In the approximation of two bound channels ($n = 1,2$) under the condition leading to equation (19)

$$u_1(\vec{r})|_{r\to\infty} = \mathrm{e}^{\mathrm{i}\vec{k}\vec{r}} + f(\vec{k}', \vec{k})\frac{\mathrm{e}^{\mathrm{i}kr}}{r}, \tag{25}$$

u_1 is the radial-dependent wavefunction of the free particle which interacts with the target that is in the ground state, $|1\rangle = \Phi_1(\xi)$, and u_2 interacts with the target that is in the bound excited state, $|2\rangle = \Phi_2(\xi)$. So, equation (25) describes the process in which the target in its ground state is excited by the flow of particles from infinity, which have momentum $\vec{k}_1$. In the case when the energy of the scattering system is close to energy of the resonant transition, that is, to eigenenergy of the discrete spectrum of the Hamiltonian $\hat{h}_2$ (24), that is, $\hat{h}_2\varphi_\lambda = E_\lambda\varphi_\lambda$ and $E \approx E_m$, the equation

$$u_1 = \psi^{(+)}_{1,\vec{k}_1}(\vec{r}) + [\hat{G}_1(E, \vec{r}, \vec{r}')V_{12}(\vec{r})\varphi_0]\frac{1}{E - E_m}\langle\varphi_0|\ V_{21}|u_1\rangle \tag{26}$$

can be solved with respect to u_1, yielding an amplitude of elastic scattering near resonance as

$$f(\vec{k}', \vec{k}) = f_{\text{pot}}(\vec{k}, k) - \frac{\mu}{2\pi\hbar^2}\frac{\langle\psi^{(-)}_{1,\vec{k}}|\ V_{12}|\varphi_0\rangle\langle\varphi_0|\ V_{21}|\psi^{(+)}_{1,\vec{k}}\rangle}{E - (E_m + \Delta) + i\dfrac{\Gamma}{2}}, \tag{27}$$

where $f_{\text{pot}}(\vec{k}, k)$ is the amplitude of the potential scattering, μ is the electron mass and Δ is the decay rate

$$\Delta = \sum_\nu \frac{|\langle\varphi_0|\ \hat{V}_{21}|\psi_\nu\rangle|^2}{E - E_\nu} + \int \frac{|\langle\varphi_0|\ \hat{V}_{21}|\psi_{1,\vec{k}'}\rangle|^2}{E - E'}\rho(k')\mathrm{d}\Omega\mathrm{d}E'$$
$$\Gamma = 2\pi\int |\langle\psi_{1,\vec{k}'}|\ \hat{V}_{21}|\varphi_0\rangle|\ \rho(k')\mathrm{d}\Omega, \tag{28}$$

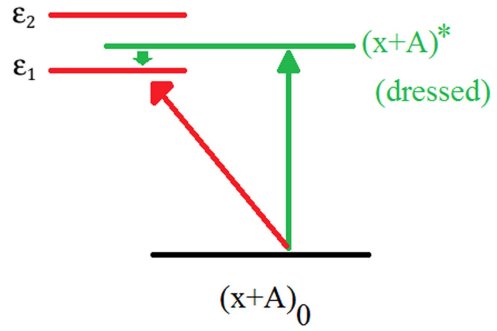

Figure 1. Level splitting in a two-channel approximation in the presence of resonance near channel-closing.

$\rho(k')$ is the density of final states, $\mathrm{d}\Omega$ is elementary solid angle, $\psi^{(+)}_{1,\vec{k}_1}(\vec{r})$ is the exact solution of the problem of elastic scattering in the case influence of all inelastic scattering channels is neglected, $\hat{G}_1(E, \vec{r}, \vec{r}')$ is Green's function, which describes movement of particle x in the channel 1 neglecting its connection to other channels, $V_{12}(\vec{r}) = V^*_{21}(\vec{r}) = \langle 1|\ \hat{V}|2\rangle = \int \Phi^*_1(\xi)\hat{V}(\xi, \vec{r})\Phi_2(\xi)\mathrm{d}\xi$, $\varphi_0 = \mathrm{e}^{i\vec{k}\vec{r}}|_{k=0}$ is the bound state of the particle, $E - E_m$ is the difference between the full energy E of the system and the energy E_i of one of eigenstates of the discrete spectrum of Hamiltonian $\hat{h}_1$. $u_2(\vec{r})|_{r\to\infty}$ is the exponentially decaying wave, which simply means that for such kinetic energies of the incident particle, the inelastic scattering can take place only virtually. ψ_ν is determined by the discrete part of spectral representation of the operator

$$\frac{1}{E^{(+)} - \hat{h}_1} = \sum_\nu \frac{|\psi_\nu\rangle\langle\psi_\nu|}{E - E_\nu} + \int \frac{|\psi_{1,\vec{k}'}\rangle\langle\psi_{1,\vec{k}'}|}{E^{(+)} - E'}\rho(\vec{k}')\mathrm{d}\Omega\mathrm{d}E'. \tag{29}$$

It should be noted that processes of excitation to elastic and inelastic states do not interfere if states E_n and E_m are not the same states of the target's Hamiltonian, because of the channel-closing condition (21). Indeed, the electron can be trapped in the elastic scattering state due to channel closing (21) only if its kinetic energy is lower than the energy difference between the ground state and inelastic scattering state. The kinetic energy of the electron at the instant of return to its origin is determined only by the instant of ionization and the time dependence of pump field. But according to the uncertainty principle $\Delta t\Delta E \geqslant \hbar$, so assuming condition $E \approx E_m$ for (26) one can never tell if the electron participates in elastic or inelastic scattering when there is no state E_m with energy lower than E_n. Fortunately, E_m can easily be produced by AC Stark splitting of the considered resonant level of the unperturbed target. So the elastic scattering population can be achieved when there is AC Stark shift in the system. In the case the population of elastic scattering state Λ is nonzero (e.g. due to laser dressing) LWI is possible if the transition $\Lambda \Leftrightarrow |n\rangle$ is permitted in the presence of the pump field which is resonant to energy difference between them. Fulfillment of these conditions can greatly increase the yield of resonant HHG for higher frequency harmonics. The most important consequence of equation (27) is that the resonant state can be split in the presence of a laser field (figure 1), where the efficient cross-section of the splitting is given by the Fano equation. It has been stated in [25] that in laser-dressed states the coherence may be nonzero, and thus LWI can be possible even in conditions of no optical coherences. So, the observation of resonant HHG can be considered as the experimental evidence of three-dimensional laser dressing of states. However, the key feature of the presented model is the possibility of the population of bound states in the process of HHG, and this feature had to be demonstrated by computer simulation. Please note that existence of such excitation in computer simulation is necessary, but not sufficient to prove the presented model.

3. Calculations

Quantum mechanical simulation was performed to ensure that the excited state can in fact be populated in HHG experiments by inelastic scattering. The main part of any HHG simulation is the solution of the time-dependent Schrödinger equation (TDSE). The complexity of wavefunctions for systems with more than two degrees of freedom was the reason to restrict most of HHG simulations to SAE problems. Nowadays there are only two ways to make a TDSE solution feasible for multi-electron systems, which are based on time-dependent density functional theory (TDDFT) and multiconfigurational time-dependent Hartree–Fock (MCTDHF) approaches, respectively. Although TDDFT calculations are much faster for large problems, they are not very convenient in the investigation of the nature of HHG because nothing can be said about which electrons actually participate in the process. Additionally, available TDDFT solution packages (Octopus [26, 27], GPAW [28]) are restricted to plane-wave basis functions, which are reliable for most solid-state physics problems, but not guaranteed to give a proper picture of ionization. So from here and throughout the article we will be using the MCTDHF approach, which not only gives a good combination of exactness of the direct TDSE solution and the speed of Hartree–Fock (HF) approximation, but also has the support of the system's splitting, not included in the HF approach.

The MCTDHF approach treats the wavefunction of multi-electronic system as

$$\Psi(Q_1, ..., Q_f, t) = \sum_{j_1=1}^{n_1} ... \sum_{j_f=1}^{n_f} A_{j_1...j_f}(t) \prod_{\kappa=1}^{f} \varphi^{(\kappa)}_{j_\kappa}(Q_\kappa, t), \tag{30}$$

where $Q_1, ..., Q_f$ are the coordinates of electrons, $A_{j_1...j_f}$ is the antisymmetrized A-vector for all n_κ time-dependent expansion functions $\phi^{(\kappa)}_{j_\kappa}$ for every degree of freedom κ. Setting $n_\kappa = n_1$ describes the direct solution of TDSE and $n_\kappa = 1$ simplifies the wavefunction to ordinary time-dependent HF approximation. For direct observations of collisional excitation of core electrons we also reduce this representation to that of the original MCTDHF approach, thus considering the A-vector as nonsymmetrized and the particles distinguishable, which modifies the electron–electron scattering cross-section only

quantitatively (due to exchange interaction). So this modification will not destroy the physical meaning of the observed processes.

The equations of motion in the MCTDHF approach are derived from the modified variational principle

$$\langle \delta\Psi_{\mathrm{MCHF}}(t) \left| i\frac{\mathrm{d}}{\mathrm{d}t} - \mathrm{H}(t)|\Psi_{\mathrm{MCHF}}(t)\right\rangle = 0 \ \forall\ t. \qquad (31)$$

We also check the choice of basis functions to ensure that the system actually supports the bound level structure and free particle movement. For the solution of MCTDHF equations of motion we use the Heidelberg MCTDH package [29–32], which has good support for various basis functions in discrete variable representation (DVR). For the description of the angular motion of electrons and dependence of pseudopotential on the orbital momentum of electrons, we use Legendre type DVR (spherical harmonics in the laser polarization plane):

$$\chi_{l-m+1}(\theta) = \sqrt{\frac{2l+1}{2}\frac{(l-m)!}{(l+m)!}}\, P_l^m \cos(\theta). \qquad (32)$$

For longitude movement of the electron, a careful choice of basis is required because ground state basis functions, which can be obtained from molecular geometry programs, have a good representation of ground-level structure and can give very good ionization dynamics and cross-sections, but they do not include support for a particle in free space. It has been shown in [33] that pseudopotentials not only reduce the computational effort, but also make plane-wave basis sets more appropriate for the real systems, so the first evident choice is the exponential DVR

$$\chi_j(x) = (|x_{\max 1} - x_{01}|)^{-1/2} \exp(2i\pi j(x - x_{01})/(|x_{\max 1} - x_{01}|)). \qquad (33)$$

We supposed that the discrete level structure can be better represented by combining these exponential DVR and Laguerre (hydrogen-like) basis functions

$$\chi_n(x) = x^{1/2}(|x_{\max 2} - x_{02}|)\sqrt{(n-1)!/n!}\exp(-x/2). \qquad (34)$$

The pseudopotentials for In ionic backgrounds have been generated by means of the OPIUM pseudopotential generator [34] for neutral, singly and doubly ionized In. Resonant HHG in In is attributed to the $4d^{10}5s^2\ {}_1S^0 \rightarrow 4d^9 5s^2 5p\ {}^1P_1$ transition in the In^+ ion [2], so only the three-electron system is sufficient for this simple case, if correct pseudopotentials are chosen. However, when there are multiple excitations, the potential changes non-adiabatically, so for example, in the case of two-particle impact excitation the Hamiltonian will have the form

$$\hat{H} = \begin{pmatrix} H_{11} H_{12} \\ H_{21} H_{22} \end{pmatrix}, \qquad (35)$$

where H_{11} is the neutral potential, H_{21} and H_{12} are the corresponding potentials for the 1st and the 2nd core electrons removed and H_{22} is the potential of both core electrons being excited. The states are electronically coupled to each other.

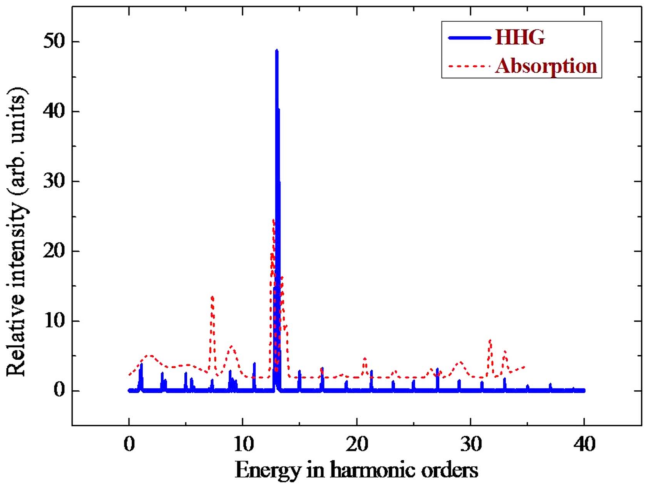

Figure 2. Absorption spectrum of a singly charged In ion (dashed line, shifted by 2 units of relative intensity for better visibility) and resonant HHG spectrum (solid line) of the full system.

The resulting HHG spectrum was obtained by Fourier transformation of the induced dipole.

As a driving pulse we used for all calculations the Gaussian-shaped linearly polarized beam with FWHM of 35 fs and carrier frequency of 0.057 au ($\lambda = 800$ nm), peak intensity 5×10^{14} W cm^{-2} and Gaussian-shaped envelope. Utilization of angular degrees of freedom for a linearly polarized pump may seem questionable, but for given pseudopotentials there is support of scattering as well, that is, change in orbital momentum of every particle may modify its energy in such a way, that scattering will in fact be more probable than direct fall in its place, which is achieved by electronic coupling of the potential energy surfaces with fixed orbital momentum to each other.

In figure 2 (dashed line), the absorption spectrum of a given system (In ion, external electron removed, that is, H_{11} pseudopotential) is presented, which has been obtained by adding an impulse to every electron in it and letting the system propagate freely for a long time (35 fs) and taking the spontaneous emission spectrum afterwards. It is seen that there are some prominent absorption peaks in the area of the 13th harmonic, which can be predicted from time-independent simulations. Then we performed propagation of the system in a laser field and obtained the corresponding results for spontaneous emission based estimate of HHG (figure 2, solid line). The cutoff was observed for the 39th harmonic and non-resonant harmonics had approximately the same intensity in the plateau region. It is actually not surprising that resonant HHG has been observed, although with the intensity only 10–20 times higher than non-resonant harmonics, which is less than that obtained from experimental studies [2–4].

To investigate the process further, we monitored the movement of all particles in the system. Notice that even in case that they were not treated as antisymmetric, but as distinguishable, even the particles not influenced by the laser have in general been transferred to excited potential surfaces. This evidently means that for some accelerated electron energy, the system would have less energy when this energy

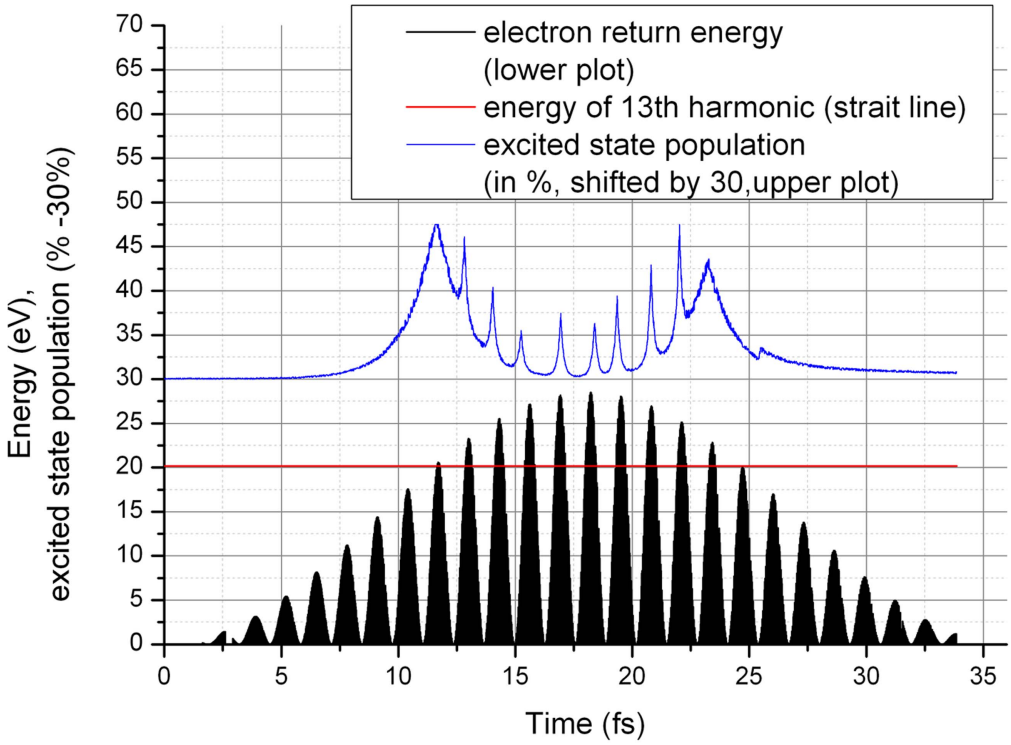

Figure 3. Time dependence of the electron return energy (black area) and the excited state population (blue line) for 35 fs pulses with Gaussian envelope; peak intensity: 5×10^{14} W cm^{-2}. The maximum excited state population reached 17.5% (upper blue line and shifted upwards by 30 units for better visibility).

is exchanged during the inelastic collision, that is, collision excitation is possible, and this excitation also happens coherently due to short pump pulses.

To check if the population transfer indeed occurs due to inelastic collision, and not some direct process or radiationless electron capture, we compared the possibility of the second particle occupying the excited state (by analyzing the indices of product functions from $l = 2$ d-ground state to $l = 1$ p-state), with the maximum kinetic energy of the accelerated particle at the instant of recombination derived from semi-classical assumptions [1]. It is clearly seen that the population of the excited state has time-dependent peaks (figure 3) with maximums close to the instants when kinetic energy at return time is in general very close to that of the resonant 13th harmonic. In contrast, if resonant HHG would originate from the accelerated particle itself (direct recombination or electron capture), these peaks for indistinguishable particles would correspond to instants when the kinetic energy at the instant of recombination is equal to the energy of resonant harmonic minus ionization energy and for distinguishable particles there should have been no clear dependence at all. It is seen that only the kinetic energy of the accelerated particle is transferred for the excitation of another one, so the collision excitation of inner electrons during inelastic scattering is possibly the base of resonant HHG. The population of the excited state also experiences some Rabi-like oscillations, which can, in principle, show the possibility LWI processes.

The population in figure 3 is normalized to 13 for better visibility, and 13 corresponds to the maximum observed occupation of excited state of approximately 17.5%, which means that there is no population inversion during the HHG process, so stimulated emission based enhancement is not possible. We can deduce then that resonant HHG is also in general a spontaneous emission.

4. Experiment

To compare the modeling of resonance enhancement with experiment the following studies were carried out, which demonstrated the enhancement of different harmonics in the vicinity of the $4d^{10}5s^2\ {}_1S^0 \rightarrow 4d^9 5s^2 5p\ {}^1P_1$ transition in the In(II) ion (19.92 eV, 62.24 nm). The gf value, the product of the oscillator strength f of a transition and the statistical weight g of the lower level, of this transition has been calculated to be $gf = 1.11$ [35], which is more than 12 times larger than that of any other transition from the ground state of In II. This transition is energetically close to the 13th harmonic ($h\nu_{H13} = 19.99$ eV or $\lambda = 62$ nm) of 806 nm radiation, the 23rd harmonic ($h\nu_{H23} = 19.93$ eV or $\lambda = 62.21$ nm) of 1431 nm radiation and the 25th harmonic ($h\nu_{H25} = 20.38$ eV or $\lambda = 60.84$ nm) of 1521 nm radiation, thereby allowing the resonance-induced enhancement of their intensity provided the plasma conditions allow maximally efficient harmonic generation.

The details of the experimental setup are described elsewhere [36]. Briefly, the experimental setup consisted of a Ti:sapphire laser, a traveling-wave optical parametric amplifier (OPA) of white-light continuum and a HHG scheme

using propagation of the amplified signal pulses from the OPA through the extended laser-produced plasma (LPP). Part of the amplified radiation with a pulse energy of 6 mJ was separated from the whole beam and used as a heating pulse for homogeneous plasma formation using a 200 mm focal length cylindrical lens installed in front of the extended (5 mm) In target placed in the vacuum chamber. We analyzed the In plasma as the medium for harmonic generation using the tunable and fixed sources of ultrashort pulses. The remaining part of the amplified radiation (806 nm, 64 fs) was delayed with regard to the heating pulse and propagated through the LPP. Another pump of plasma were the signal pulses from the OPA. The signal pulses from the OPA allowed tuning along the 1200–1600 nm. As it was mentioned above, we used the 1431 and 1521 nm pumps (70 fs). These driving pulses were focused at a distance of ~150 μm above the target surface. The plasma and harmonic emissions were analyzed using an extreme ultraviolet spectrometer.

Our experiments were carried out using both the single-color (806 nm) and two-color (1431 nm + 715.5 nm, 1521 nm + 760.5 nm) pumps of the LPP. The reasons for using the double-beam configuration to pump the extended plasma is related to the small energy of the driving mid-infrared (MIR) signal pulses (<1 mJ). The $I_H \propto \lambda^{-5}$ rule (I_H is the harmonic intensity and λ is the driving field wavelength [37]) led to a significant decrease of harmonic yield in the case of longer-wavelength sources compared with the 806 nm pump and did not allow the observation of strong harmonics from the single-color MIR (1431 nm or 1521 nm) pulses. Because of this we used the second-harmonic (H2) generation of the signal pulse to apply the two-color pump scheme (MIR + H2) for plasma HHG. A 0.5 mm-thick beta barium borate crystal was installed inside the vacuum chamber on the path of focused signal pulse. The conversion efficiency of 715.5 nm and 760.5 nm pulses was ~15%. The two orthogonally polarized pump pulses were sufficiently overlapped both temporally and spatially in the extended plasma, which led to a significant enhancement of odd harmonics, as well as generation of even harmonics of similar intensity as the odd ones.

The upper panel of figure 4 shows the plasma emission spectrum of In plasma at the conditions of ablation, which do not allow efficient HHG. The harmonics generated in the In plasma when plasma emission was suppressed due to lower fluence of heating pulses. The three bottom panels correspond to the latter conditions. In the case of the 806 nm pump (second panel from the top), the extremely strong 13th harmonic (H13) dominated the whole spectrum of emission. This harmonic was close to the 62.24 nm transition of In(II) shown as the solid line. H13 was 15 to 40 times stronger than the neighboring harmonics depending on the plasma formation conditions.

The use of the two-color pump of MIR pulses (1431 nm + 715.5 nm, third panel from the top) also demonstrated the enhancement of harmonics in the vicinity of the 62.24 nm transition of the In ion. One can see the enhancement of odd and even harmonics close to this wavelength. H23 exactly matched with the above resonance transition and

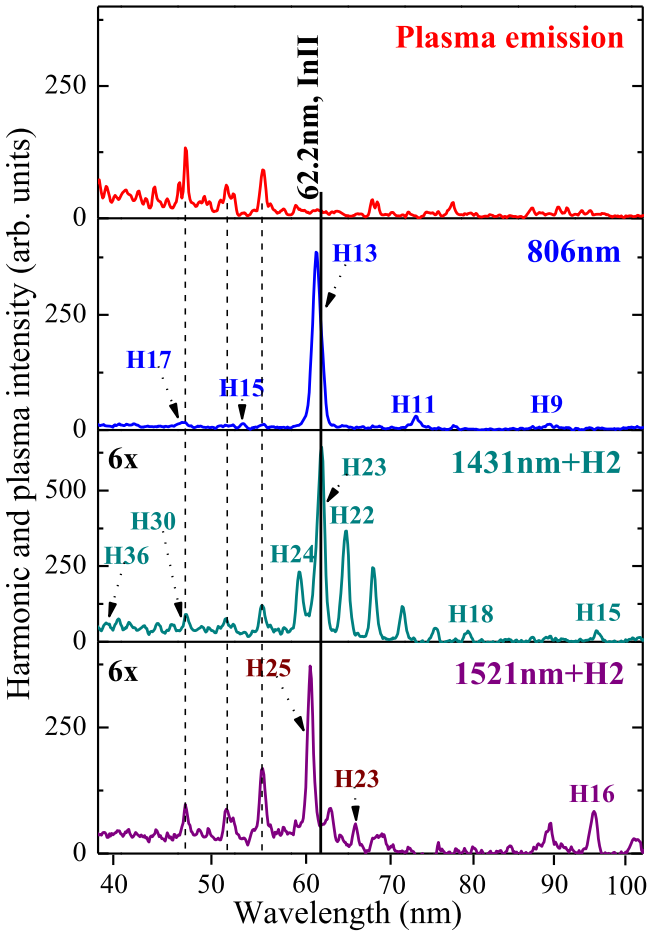

Figure 4. Plasma and harmonic emission spectra generating in the In plasma. Upper panel: plasma emission at over-excitation of ablating target. Second panel: single-color pump (806 nm) of optimally formed In LPP. Third panel: two-color pump (1431 nm + 715.5 nm) of optimally formed In LPP. Fourth panel: two-color pump (1521 nm + 760.5 nm) of optimally formed In LPP. The two bottom panels were magnified with the factor of 6× compared with the second panel due to the notably smaller conversion efficiency in the case of longer-wavelength pumps. Solid line corresponds to the InII transition responsible for the enhancement of harmonics. Dotted lines show the emission lines of In plasma observed in all these cases.

correspondingly showed the highest yield. In the case of another two-color pump (1521 nm + 760.5 nm, fourth panel from the top) the optimal conditions of the most efficient conversion were maintained for the H25.

Thus, the transition of In(II) significantly affected the harmonic spectrum generating from the In LPP. Notice that the application of most other targets did not lead to the enhancement of specific harmonic but rather to the featureless homogeneous harmonic distribution gradually decreasing up to the cut-off region. These studies confirmed the earlier reported studies on the significant influence of some ionic transitions on the harmonic distribution, which were also observed in the case of Cr, Mn, Sn and some other plasmas. The enhancement factors of specific harmonics noticeably depended on the oscillator strengths of the involved ionic transitions. Note that in some cases the conditions for resonant recombination were fulfilled for

more than one harmonic provided two-color fields were used. So there should not be a single resonance populated during HHG. Any multiphoton-based resonant excitation cannot explain such multiple resonant enhancement, while our approach for resonant HHG excitation by inelastic scattering remains valid as inelastic scattering channels of different spectral terms (here $4d^{10}5s^x5p^y \rightarrow 4d^95s^x5p^{y+1}$) can be populated by accelerated electron with probability proportional to square of oscillator strength. The radiation of harmonics is also the stimulated emission as resonant HHG greatly decreased at conditions of spectral detuning of MIR pulses from resonances. The lifetime of the resonant state is also much greater than the duration of both the main pulse and resulting harmonics considering a significant spontaneous emission at the harmonic frequency of an important process. It has been shown both theoretically and experimentally for In [35], Sn [38], Sb [39], Cr [40] that electronic transitions from the inner d-subshell to outer p-subshell (that corresponds to the subshell where the first detached electron originally resided) of species with different ionization degrees lie close to each other. Control of degree of ionization of laser plasma can thus be used to fine-tune the frequencies of harmonics, which can be resonantly generated. The model of multi-electron resonant recombination restricts the choice of spectral transitions, which are promising to resonant HHG to permit dipole transitions from the inner subshells to the lowest unoccupied subshell.

Similar results which show resonant enhancement can be obtained using some fixed model potential e.g. described in [17]. However, the potential [17] has two major drawbacks, one resulting from another (1) this is a fitting potential which has no obvious physical explanation or direct relation to certain spectral transition lines (2) it cannot be calculated *ab initio* or derived from any theoretical assumption or approximation for a given system, all four parameters can be fitted only using the experimental data. So, in fact its precision is a result of fitting to an experiment. The theory presented in [17] is quite precise and describes many experimentally observed features of resonant HHG in given systems which makes it really valuable. But it has little relation to the described potential barrier. In contrast, the matrix transition element is a core part of our model. So the resulting estimates of equation (6) in [17] can be even better confirmation for our model than for that of the fixed potential.

One should be very careful when speaking of precise coincidence of theoretical and experimental quantitative results. There is a problem of reproducibility of probe beam—experimental results are mostly averaged over shots, while in theory and calculations the laser beams tend to be perfect Gaussian beams. There is also a problem of phase matching which relates to the concentration of laser-ablated plasma particles. The concentration of laser plasma is in fact very difficult to calculate. In addition, in most calculations the ablation beam itself is also not exactly reproducible. Every theory inflicts additional approximation errors. This all should be considered when respecting precision of calculation as the best proof for validity of theory. But the model potential in [17] has the immense advantage of reducing a multi-electron problem to a one-electron problem. So better binding of its parameters to spectral properties of given systems can be considered promising as well.

As for derivation of equation (6) in [17] one should note that no relaxation-related process is actually included. In contrast, the analytical model of equation (6) considers only some of the population of a reaction channel, and even in [17] this channel is viewed as an inelastic scattering channel. To sum it up, our model is in fact supported by the calculations given in [17], and some possible difference in modeling is not too important.

5. Conclusions

In conclusion, the 4-step analytical model of resonant enhancement of HHG was extended to real systems with resonant transitions of inner-shell electrons. Resonant enhancement was explained by LWI in a three-level system of ground, excited and shifted resonant scattering states which are coupled to the fundamental field and its high harmonics. The role of inelastic scattering was studied by simulation of the excited state's population dynamics. It was shown that maximal gain is achieved when the energy shift between the excited state and resonant scattering state is close to the energy of the photon of the fundamental field. The multi-electron resonant recombination model assumes excitation of inner electrons to resonant levels of the system by inelastic cross-section. Calculations show that the resonant level is populated in the HHG process by inelastic scattering. A combination of populated excited state and resonant elastic scattering state coupled to the main pump can lead to resonant HHG enhancement by the LWI process. Resonant HHG can be considered as experimental evidence of three-dimensional laser dressing of states. We have demonstrated the enhancement of harmonics in the In plasma using different pumps. Particularly, the 13th, 23rd and 25th harmonics were notably enhanced compared with the neighboring harmonics using the 806, 1431 and 1521 nm pumps.

Acknowledgments

We thank H Kuroda and M Suzuki for their support during these studies.

ORCID iDs

P V Redkin https://orcid.org/0000-0002-7436-5614
R A Ganeev https://orcid.org/0000-0001-5522-1802

References

[1] Corkum P B and Krausz F 2007 Attosecond science *Nature Phys.* **3** 381

[2] Ganeev R A, Suzuki M, Baba M, Kuroda H and Ozaki T 2006 Strong resonance enhancement of a single harmonic generated in the extreme ultraviolet range *Opt. Lett.* **31** 1699
[3] Ganeev R A, Suzuki M, Baba M and Kuroda H 2005 Harmonic generation from chromium plasma *Appl. Phys. Lett.* **86** 131116
[4] Ganeev R A, Suzuki M, Redkin P V, Baba M and Kuroda H 2007 Variable pattern of high-order harmonic spectra from a laser-produced plasma by using the chirped pulses of narrow-bandwidth radiation *Phys. Rev.* A **76** 023832
[5] Faria F M C, Copold R, Becker W and Rost J M 2002 Resonant enhancements of high-order harmonic generation *Phys. Rev.* A **65** 023404
[6] Taieb R, Veniard V, Wassaf J and Maquet A 2003 Roles of resonances and recollisions in strong-field atomic phenomena: II. High-order harmonic generation *Phys. Rev.* A **68** 033403
[7] Pfeifer T, Gallmann L, Abel M J, Neumark D M and Leone S R 2006 Single attosecond pulse generation in the multicycle-driver regime by adding a weak second-harmonic field *Opt. Lett.* **31** 975
[8] Zeng Z, Li R, Cheng Y, Yu W and Xu Z 2002 Resonance-enhanced high-order harmonic generation and frequency mixing in two-color laser field *Phys. Scr.* **66** 321
[9] Andreev A V, Stremoukhov S Y and Shoutova O A 2013 High-order optical harmonic generation in ionization-free regime: origin of the process *J. Opt. Soc. Am.* B **30** 1794
[10] Corkum P B 1993 Plasma perspective on strong-field multiphoton ionization *Phys. Rev. Lett.* **71** 1994
[11] Plaja L and Roso L 1993 High-order harmonic generation in a two-level atom *J. Mod. Opt.* **40** 793
[12] Gaarde M and Schafer K 2001 Enhancement of many high-order harmonics via a single multiphoton resonance *Phys. Rev.* A **64** 013820
[13] Plummer M and Noble C J 2002 Resonant enhancement of harmonic generation in argon at 248 nm *J. Phys. B: At. Mol. Opt. Phys.* **35** L51
[14] Ishikawa K 2003 Photoemission and ionization of He^+ under simultaneous irradiation of fundamental laser and high-order harmonic pulses *Phys. Rev. Lett.* **91** 043002
[15] Oleinikov P A, Platonenko V T and Ferrante G 1994 Resonant generation of high harmonics *J. Exp. Theor. Phys. Lett.* **60** 246
[16] Milosevic D B 2007 High-energy stimulated emission from plasma ablation pumped by resonant high-order harmonic generation *J. Phys. B: At. Mol. Opt. Phys.* **40** 3367
[17] Strelkov V 2010 Role of autoionizing state in resonant high harmonic generation and attosecond pulse production *Phys. Rev. Lett.* **104** 123901
[18] Mompart J and Corbalán R 2000 Lasing without inversion *J. Opt. B: Quantum Semiclass. Opt.* **2** R7
[19] Kopold R, Becker W, Kleber M and Paulus G G 2002 Channel-closing effects in high-order above-threshold ionization and high-order harmonic generation *J. Phys. B: At. Mol. Opt. Phys.* **35** 217
[20] Paulus G G, Grasbon F and Walther H 2001 Channel-closing-induced resonances in the above-threshold ionization plateau *Phys. Rev.* A **64** 021401 (R)
[21] Redkin P V and Ganeev R A 2010 Simulation of resonant high-order harmonic generation in a three-dimensional fullerenelike system by means of a multiconfigurational time-dependent Hartree–Fock approach *Phys. Rev.* A **81** 063825
[22] Balashov V V 2012 *Quantum Scattering Theory* (Moscow: MAKS press) (nuclphys.sinp.msu.ru/qti/balashov.pdf)
[23] Ganeev R A, Elouga Bom L B, Abdul-Hadi J, Wong M C H, Brichta J-P, Bhardwaj V R and Ozaki T 2009 Higher-order harmonic generation from fullerene by means of the plasma harmonic method *Phys. Rev. Lett.* **102** 013903
[24] Ganeev R A, Elouga Bom L B, Wong M C H, Brichta J-P, Bhardwaj V R, Redkin P V and Ozaki T 2009 High-order harmonic generation from C_{60}-rich plasma *Phys. Rev.* A **80** 043808
[25] Agarval G S 1991 Origin of gain in systems without inversion in bare or dressed states *Phys.Rev.* A **44** R28
[26] Marques M A L, Castro A, Bertsch G F and Rubio A 2003 Octopus: a first principles tool for excited states electron–ion dynamics *Comp. Phys. Comm.* **151** 60
[27] Castro A, Appel H, Oliveira M, Rozzi C A, Andrade X, Lorenzen F, Marques M A L, Gross E K U and Rubio A 2006 Octopus: a tool for the application of time-dependent density functional theory *Phys. Stat. Sol.* (b) **243** 2465
[28] Mortensen J J, Hansen L B and Jacobsen K W 2005 Real-space grid implementation of the projector augmented wave method *Phys. Rev.* B **71** 035109
[29] Beck M H, Jackle A, Worth G A and Meyer H-D 2000 The multiconfiguration time-dependent Hartree (MCTDH) method: a highly efficient algorithm for propagating wavepackets *Phys. Rep.* **324** 1
[30] Meyer H-D, Manthe U and Cederbaum L S 1990 The multi-configurational time-dependent Hartree approach *Chem. Phys. Lett.* **165** 73
[31] Manthe U, Meyer H-D and Cederbaum L S 1992 Wave-packet dynamics within the multiconfiguration Hartree framework: general aspects and application to NOCl *J. Chem. Phys.* **97** 3199
[32] Meyer H-D and Worth G A 2003 Quantum molecular dynamics: propagating wavepackets and density operators using the multiconfiguration time-dependent Hartree (MCTDH) method *Theor. Chem. Acc.* **109** 251
[33] Fuchs M and Scheffler M 1999 *Ab initio* pseudopotentials for electronic structure calculations of poly-atomic systems using density-functional theory *Comp. Phys. Commun.* **119** 67
[34] Grinberg I, Ramer N J and Rappe A M 2000 Transferable relativistic Dirac–Slater pseudopotentials *Phys. Rev.* B **62** 2311
[35] Duffy G and Dunne P 2001 The photoabsorption spectrum of an indium laser produced plasma *J. Phys. B: At. Mol. Opt. Phys.* **34** L173
[36] Ganeev R A, Wang Z, Lan P, Lu P, Suzuki M and Kuroda H 2016 Indium plasma in the single- and two-color mid-infrared fields: enhancement of tunable harmonics *Phys. Rev.* A **93** 043848
[37] Lan P, Takahashi E J and Midorikawa K 2010 Wavelength scaling of efficient high-order harmonic generation by two-color infrared laser fields *Phys. Rev.* A **81** 061802
[38] Duffy G, van Kampen P and Dunne P 2001 4d $\rightarrow$ 5p transitions in the extreme ultraviolet photoabsorption spectra of Sn II and Sn III *J. Phys. B: At. Mol. Opt. Phys.* **34** 3171
[39] D'Arcy R, Costello J T, McGuinness C and O'Sullivan G 1999 Discrete structure in the 4d photoabsorption spectrum of antimony and its ions *J. Phys. B: At. Mol. Opt. Phys.* **32** 4859
[40] McGuinness C, Martins M, van Kampen P, Hirsch J, Kennedy E T, Mosnier J-P, Whitty W W and Costello J T 2000 Vacuum–UV absorption spectrum of a laser-produced chromium plasma: 3p-subshell photoabsorption by Cr^{2+} ions *J. Phys. B: At. Mol. Opt. Phys.* **33** 5077